ADVANCED FUNCTIONAL MATERIALS
www.afm-journal.de

High-Rate Continuous Synthesis of Nanocrystalline Perovskites and Metal Oxides in a Colliding Vapor Stream of Microdroplets

*Teyeb Ould-Ely, Lyle Kaplan-Reinig, and Daniel E. Morse**

A high-rate, continuous synthesis of functional nanomaterials using a home engineered reactor is reported. The reactor is able to produce low-cost, kilogram-scale $BaTiO_3$ nanopowders with a nanocrystalline particle size less than 30 nm at mild temperatures (<100 °C) and ambient pressure. Nebulization and collision of warm microdroplets (60–80 °C) of $Ba(OH)_2$ and $Ti(O\text{-}nBu)_4$ very quickly result in total hydrolysis and subsequent conversion to $BaTiO_3$, yielding 1.3 kg/day of high purity, highly crystalline nanoparticles (25–30 nm). This synthesis procedure also enables high-rate production of TiO_2 anatase (2.9 kg/day). It therefore provides a general platform for processing and scaling up of functional inorganic nanomaterials under very mild conditions.

1. Introduction

Advances in technology are driving the need for more efficient and cost-effective scaled-up production of functional nanomaterials.[1] The lack of a workforce trained for scale-up and process control of nanomaterials manufacturing, the gap between laboratories and economically practical nanofabrication and the funding strain on the survivability of start up companies all contribute to the difficulties in scaling up nanotechnologies and their commercialization.

Dr. T. Ould-Ely, Dr. D. E. Morse
Institute for Collaborative Biotechnologies
University of California
Santa Barbara, California, 93106–5100, USA
E-mail: d_morse@lifesci.ucsb.edu
Dr. T. Ould-Ely, Dr. D. E. Morse
California NanoSystems Institute
University of California
Santa Barbara, California, 93106–5100, USA
Dr. T. Ould-Ely, Dr. D. E. Morse
Materials Research Laboratory
University of California
Santa Barbara, California, 93106–5100, USA
Dr. T. Ould-Ely, Dr. D. E. Morse
Department of Molecular
Cellular and Developmental Biology
University of California
Santa Barbara, California, 93106–5100, USA
Dr. T. Ould-Ely, L. Kaplan-Reinig, Dr. D. E. Morse
LifeCel Technology, Inc.
Santa Barbara, CA, 93106–5080, USA

DOI: 10.1002/adfm.201301916

From an engineering perspective, maintaining fidelity of the original properties of nanomaterials, consistency from batch to batch, and affordability pose many challenges hindering the achievement of commercial scale production of nanomaterials.[2,3] The National Science and Technology Council of the US pointed out that general lack of safe, cost-effective nanomanufacturing and process control for advanced materials are the key impediments to nanotechnology.[1,4] Several recent projects funded by the US and EU[5] dealing exclusively with large-scale production of nanomaterials are focused on the necessity for new solutions for cost-effective nanomaterials production in quantities that can realistically lead to commercial applications.[6,7]

We have tackled this issue using a kinetically controlled vapor diffusion concept inspired by nature.[8–10] Previously, we demonstrated the feasibility of this approach with the scaled-up synthesis of barium titanate nanocrystalline particles in a batch reactor.[11]

We report here a high rate continuous synthesis of functional inorganic nanomaterials using colliding vapor stream of reagents microdroplets. This technique affords kilogram scale nanomanufacturing of sub-30 nm $BaTiO_3$ at neutral pH, atmospheric pressure, and at temperature below 100 °C. Furthermore, we show that our engineered vapor collision approach provides a generic platform for scaling up a variety of other nanomaterials.

Barium titanate is selected since, in batch mode, we identified the critical parameters that must be controlled to achieve cost-effective scale-up of synthesis with preservation of the desired properties of the resulting nanocrystals.[11,12] Furthermore, $BaTiO_3$, is a critical material for many advanced technological applications due to its exceptionally large piezoelectric compliance, pyroelectric coefficients, dielectric susceptibilities and electro-optic properties. These assets make $BaTiO_3$ a very attractive material for advanced nanotechnological applications, such as high energy density capacitors,[13] pyroelectric thermal imaging devices,[14] gate insulators in transistors, electro-optic light valves, multiferroic transducers, energy harvesters,[15] CO_2 capture and sequestration,[16] cloaking,[17] positive temperature coefficient resistors (PTCRs),[12,18] thin-film memory elements, electrocaloric coolers for computers,

phased-array radar and capacitive memory cells for electric motor vehicles.[19–22]

Conventionally, $BaTiO_3$ particles are prepared via a solid-state reaction from the calcination of $BaCO_3$ and TiO_2. The as-prepared powder is typically coarse, extensively agglomerated and its synthesis energetically costly (requiring temperatures >1000 °C). Hydrothermal, sol–gel, and co-precipitation methods have been widely investigated,[23–26] but these techniques often require harsh conditions (high concentrations of alkali or acid, and thermal processing at temperature >100 °C).

Dry methods such as spray pyrolysis[27] and combustion methods also have been reported, but the high temperatures (typically >300 °C)[28] of these processes preclude in situ functionalization with soft materials such as enzymes and polymers. Furthermore, the grain size obtained is generally large (>50 nm) and the resulting particles are severely agglomerated.

With the need for miniaturization, densification and surface functionalization of $BaTiO_3$ nanoparticles in the sub-30 nm regime, synthesis under mild conditions (neutral pH and <100 °C temperature) is highly desired. In the sub-30 nm regime, $BaTiO_3$ nanoparticles tend to sinter at much lower temperature than required for larger particles, potentially saving time and energy in the production of dense dielectric ceramics. Densification is typically required for multilayered ceramics and ultrathin PTCR thermistors, as it provides greater strength per unit thickness and increased resistance to dielectric breakdown. Furthermore, in this size regime the nanoparticles are generally single domain and thus useful for superparaelectric applications.[29,30]

2. Results and Discussion

While a few promising wet-chemical synthesis approaches produce sub-30 nm particles of $BaTiO_3$, in batch-mode[11,31–34] they have yet to prove their suitability for commercialization. The synthesis reported here employs a home-made continuous-flow reactor, fed with very low cost reagents realistically suitable for large-scale deployment and commercialization. This nanomanufacturing reactor is described in **Figure 1** (for additional details see Figure 1S).

We start with two relatively inexpensive reactants: $Ti(O\text{-}nBu)_4$ (0.15 M in H_2O) and $Ba(OH)_2$ (0.15 M in 2-propanol with 1% (v/v) oleyl alcohol). The continuous-flow reactor uses 2 ultrasonic nebulizers to produce colliding sprays of microdroplets (11.8 μm diam.) containing these warmed (80 °C) reactants. Hydrolysis, polycondensation, and quantitative conversion to $BaTiO_3$ occurs virtually instantaneously, producing 0.959 g/min (1.3 kg per 24 h) of white nanocrystalline powder of $BaTiO_3$ as demonstrated by transmission electron microscopy (TEM) and X-ray diffraction (XRD) (**Figure 2**).

The presence of oleyl alcohol (or other long chain alcohols >C4) ensures rapid functionalization and stabilization of the product nanoparticles; in the absence of such a stabilizer, shapeless particles with high polydispersity were observed. While the longer chain-lengths exhibited better confinement of nanocrystalline growth, their poor miscibility with water led in some cases to impurities ($Ba(OH)_2$ and $Ti(OH)_4$). Additions of only 1% (v/v) 2-octanol or oleyl alcohol) were optimal for confining nanoparticle growth without compromising miscibility, yielding a final product with >99% freedom from impurities.

To investigate the effect of solvent chain length, we kept all nanofabrication parameters constant; these included droplet size of 11.8 μm with a wide spray angle, temperature at 80 °C and precursor concentrations of 0.15 M. Incorporation of either long-chain alcohol significantly improved the dispersion of the final nanoparticulate powder, although the particle sizes remained in the 25–30 nm range. Qi et al. recently demonstrated strong effects of solvent chain-length in batch mode synthesis.[33]

Concentration appears to significantly govern particle size, since samples collected 5 min after the start of synthesis (before reaching steady state) were only ~14 nm, while product collected 5 min after steady-state was reached were ~24 nm. XRD and TEM analyses of product collected as a function of time confirm that particle growth stabilizes at around 23–24 nm after steady-state is reached (**Figure 3**).

For our investigation into the effect of droplet size on particle growth, we selected the solvent system that displayed the best particle distribution and dispersion: 2-propanol with 1% (v/v) oleyl alcohol. Preliminary results revealed only a small effect of droplet size when the latter was changed from 11.8 μm to 26 μm. Droplet size in the range of 26 μm led to a particle size of 27 nm, while droplet size of 11.8 μm led to particles of 24 nm. Further investigation of the rates and dynamics of droplet collision and fragmentation, and further tuning of droplet size in the nano-regime, may lead to a better understanding of the control of reaction dynamics and the resulting effects on the relative rates of nucleation and growth of the nanocrystalline particles.

The mechanism of microdroplet-mediated formation of nanocrystalline $BaTiO_3$ is readily understood.[28] Hydrolysis of titanium alkoxide in microdroplets at ca. 80 °C occurs instantaneously when mixed with microdroplets of water containing solvated Ba^{+2} ions. Fragmentation and flattening of the colliding microdroplets creates a high surface area, rapidly augmenting supersaturation in the liquid as the result of accelerated evaporation; this in turn accelerates nucleation, precipitation and growth of the nanocrystalline $BaTiO_3$.[28] We note that the differential effects on nucleation and growth under these conditions actually favor growth of larger particles than those we produced in batch mode.[11]

The particles crystallize in the pseudo-cubic phase but are readily convertible to tetragonal phase upon mild sintering to 400 °C for 2 h as confirmed by Raman spectroscopy (see Supporting Information). Further sintering to 1050 °C for 30 min yields fine grains in the 100–150 nm size range (**Figure 4**).

The as-synthesized nanopowders (centrosymetric cubic Pm3m phase) before sintering display, as expected, weak permittivity and loss tangent of 7–10 and 0.05, respectively, at 2.64 GHz (**Figure 5**). The loss tangent increases to ~0.1 at the high frequency of 10.82 GHz.

The nanomaterial sintered at 1050 °C for 30 min displays a permittivity of ~80–100 and loss tangent of ~0.1 at 2.64 GHz. The permittivity and loss remain nearly the same at 10.82 GHz. This weak permittivity is possibly due to heterogeneity in the sintered pellets (resulting either from pores or a thin shell of a highly absorbing phase).[37,38]

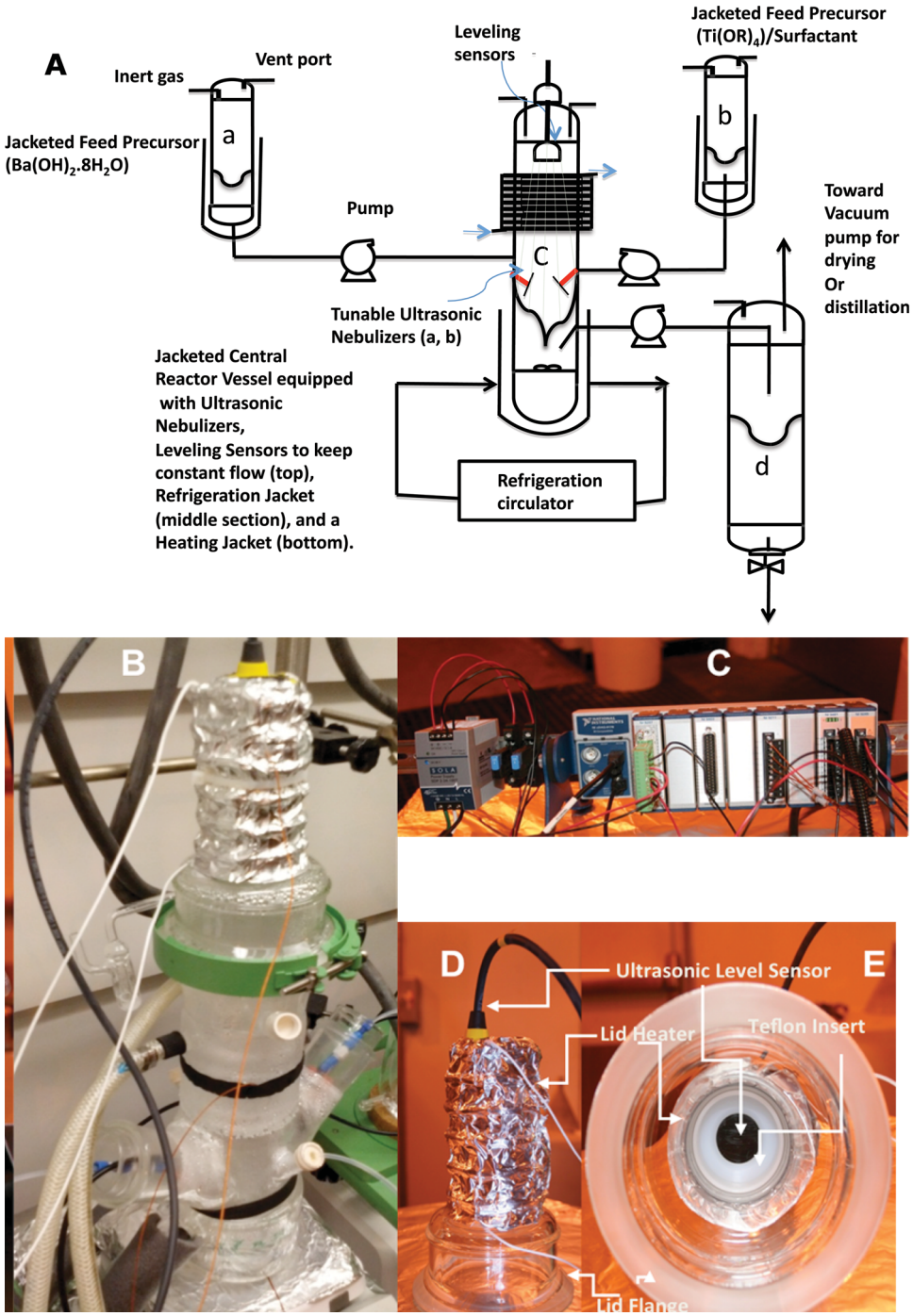

Figure 1. A) Nanomanufacturing reactor composed of: a,b) two feeding reservoirs each of 1.5 L, c) main reactor chamber (0.350 L) equipped with an internal reflux condenser, and six ports; two ports to hold the ultrasonic nebulizers to deliver a mist with tuneable droplet size, one port to hold the leveling sensor, two ports for inert gas supply, and one port for product extraction with a receiver with a capacity of 3 L. B) Close-up photograph of the main reactor. C) Photograph of the data acquisition system (DAQ) that connects to a computer for operations control and data acquisition with LabVIEW via USB. D,E) The reactor lid showing the attached ultrasonic level sensor and electric heater: D) side view of reactor lid; E) bottom view.

To verify the role of the intrinsic basicity of $Ba(OH)_2$ on the kinetics of hydrolysis and crystallization, we carried out the nanofabrication process using $BaTi(OR)_6$ and pure n-butanol or a mixture of 2-methoxy-propanol and butanol as solvents. Under these conditions, the particle size was in the range of 10–14 nm (Supporting Information, Figure 8S). However, the reaction under these conditions was very slow, requiring the use of additional aging at 80 °C in a jacketed Plug-Flow

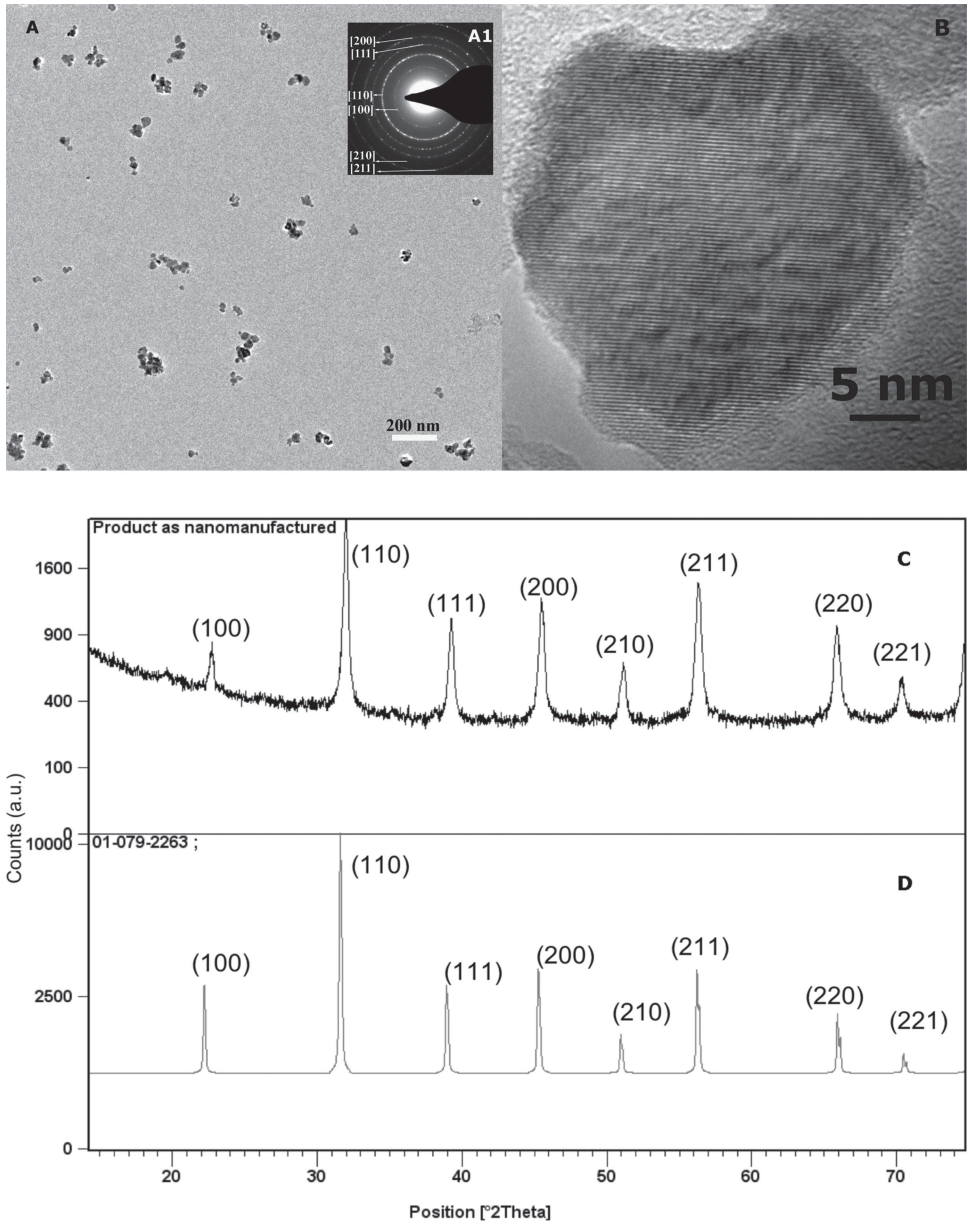

Figure 2. A) TEM showing highly crystalline $BaTiO_3$ nanoparticles (22–28 nm) synthesized in continuous flow mode, washed with alcohol and dried under vacuum. The sample was prepared for TEM by suspending the nanoparticles in EtOH. A1) Selected area diffraction pattern (SAED) confirming the high crystallinity of single-phase $BaTiO_3$. B) High-resolution image showing the high crystallinity of the nanoparticles. C) XRD pattern confirming the identity of cubic $BaTiO_3$ corresponding to JCPDS (00–079–2263) (D). Average particle size estimated to be ~23 nm from the Scherrer equation and the (110) diffraction peak.

attachment to accelerate and complete the crystallization in continuous-flow mode.

To further confirm the necessity of an intrinsic catalyst of hydrolysis, we investigated the continuous flow nanofabrication of TiO_2 using $Ti(O\text{-}nBu)_4$ alone. Under these conditions we obtained regular amorphous spheres of about 60–80 nm, suggesting the need for a catalyst. In the $BaTiO_3$ system, the intrinsic basicity of $Ba(OH)_2$ provides the catalysis needed to accelerate hydrolysis leading to the subsequent polycondensation and crystallization.

The amorphous 60–80 nm spherical particles of TiO_2 display a relatively large surface area of ~184 m^2/g as confirmed by BET measurement (see Supporting Information). Upon calcination these spheres are converted to pure, crystalline TiO_2 in the anatase polymorph (**Figure 6**). As expected, the surface area is reduced to 81 m^2/g upon calcination to 400 °C. In this case we were able to produce ~2.9 kg/24 h of amorphous titania nanospheres readily convertible to the anatase TiO_2 by calcination (Figure 6).The yield achieved in both TiO_2 and $BaTiO_3$ is summarized in **Table 1** below.

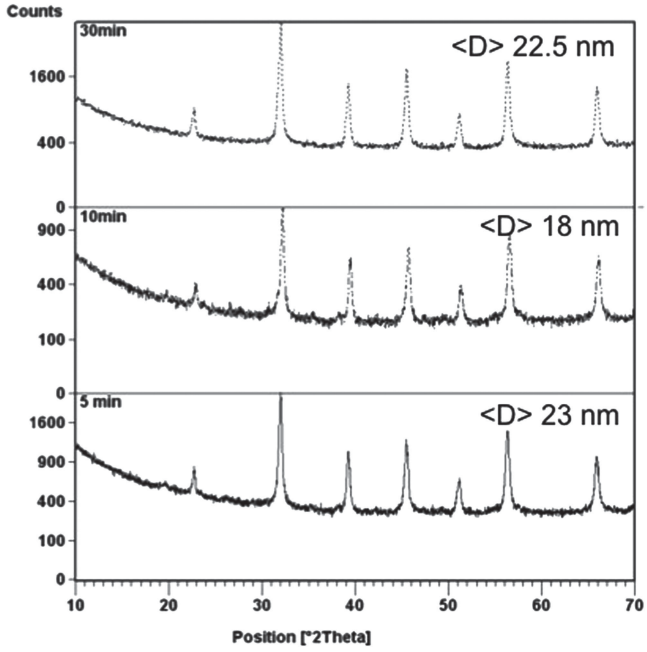

Figure 3. XRD of the product after reaching steady state; the average particle size is 23 nm for sample taken 5 min after steady state, 18 nm for sample collected after 10 min and 22.5 for sample collected after 30 min, after which the growth stabilizes at 23–24 nm. The particle size was estimated from the Scherrer equation and the (110) peak.

3. Conclusions

We report here an engineered automated continuous flow nanomanufacturing reactor yielding kg-scale of various nanocrystalline materials. This reactor could easily be translated into a still larger high-throughput ton-scale reactor. Although the continuous flow reactor also performs well with a bimetallic alkoxide used as precursor for $BaTiO_3$ nanocrystal synthesis,[11] we show here that the cost of synthesis can be significantly reduced by using the less expensive precursors, $Ti(O\text{-}nBu)_4$ and $Ba(OH)_2$).[36] We identified the microdroplet size regime in which the product size is not strongly dependent, and where it may be readily possible to replace the ultrasonic nebulizers with very inexpensive gas nebulizers while maintaining high quality in terms of purity, size and crystal structure. The possibility to recycle the solvent, integrate soft polymeric or biological functionalities (including biopolymers, peptides and enzymes) and direct processing to yield crack-free films without the need for further drying or re-dispersion also is envisioned.[35] These assets make this high rate synthesis attractive in terms of its cost, consistency of performance and compatibility with in situ functionalization requirements. Finally, to our knowledge, this is the first continuous-flow wet-chemical method for kg-scale production of small $BaTiO_3$ nanoparticles (<30 nm) under mild conditions (<100 °C). This process also afforded kg-scale synthesis of spherical sponge-like porous titania nanoparticles. Currently, we are hydrogen doping TiO_2 nanostructures to make black mesoporous titania nanosponges and investigating their photocatalytic properties.[39,40]

The reactor described here could be used to generate ternary and quaternary phases by collision of streams delivering either two different bimetallic alkoxide precursors or one bimetallic and one monometallic precursor. This process is suitable for achieving homogenous mono or multispecies doping. The reactor also could easily be reconfigured to incorporate multiple nozzles either to further increase yield or to explore new frontiers in product chemistry and composition.

We are currently installing high-speed, high-resolution cameras to dynamically image, track and understand some of the dynamic phenomena involved and responsible of accelerating the hydrolysis and crystallization processes; these include droplet collision, fragmentation and reshaping, fast evaporation, hydrolysis, nucleation-precipitation, and crystallization.

4. Experimental Section

Reagents: $Ba(OH)_2/H_2O$ 0.15 M was acquired from Aldrich, dry and stored under N_2, 2-propanol was acquired from Aldrich, $Ti(O\text{-}nBu)_4$ 0.15 M was acquired from Gelest, Oleyl Alcohol was acquired from Aldrich, Distilled water (MilliQ water, 18 mega ohm-cm), and Argon (99.99%) was acquired from Praxair.

Equipment Setup: Reactor components were assembled as shown (Figure 1A and 1S) purged with argon (99.99%, Praxair) three times; and the reagents loaded under argon as described in the section below.

High-Rate Synthesis of $BaTiO_3$ Nanomaterials in Colliding Vapor Stream of Microdroplets: 1.5 L of aqueous 0.15 M $Ba(OH)_2$ were loaded under argon in reservoir (Figure 1A) and bubbled with argon for 10 min to remove all traces of carbon dioxide and air. Carbon dioxide may lead to barium carbonate, and therefore must be avoided. 1.5 L of 0.15 M of $Ti(O\text{-}nBu)_4$ in 2-propanol with oleyl alcohol 1% (v/v) were loaded in reservoir (b) while keeping the solution under argon. 0.3–0.35 L of pure 2-propanol were loaded in the main reactor chamber. To minimize the presence of CO_2 in the central reactor, argon was bubbled for 10 min in (a), (b), and (c) while warming all jackets with circulating water to 80 °C. Both $Ba(OH)_2$ and $Ti(O\text{-}nBu)_4$ were pumped simultaneously through the nebulizers at a flow rate of 20 mL/min.The crystallized product was extracted at a flow rate of ~40 mL/min as needed to maintain a constant value in the reactor. The steady state was reached after ~22–30 min, as expected from the three residence-times (3θ) rule of thumb[36] and confirmed by our observations. Small volume samples were collected under argon 5, 10, and 30 min after steady state and rapidly dried under vacuum (10^{-2} Torr) at room temperature.

High-Rate Synthesis of TiO_2 Nanomaterials in Colliding Vapor Stream of Microdroplets: The synthesis of TiO_2 was carried out in the same manner as $BaTiO_3$. The only difference was that reservoir(a) was filled with DI water only and $Ti(O\text{-}nBu)_4$ was set at a concentration of 1 M (in 2-propanol 99%(v/v) with 1% (v/v) oleylalcohol). The final product was dried under vacuum (10^{-2} Torr) at room temperature leading to yield summarized in the Table 1. When pure 2-propanol was used, high purity, highly crystalline $BaTiO_3$ was obtained. However, the nucleation and growth of the resulting nanoparticles were poorly controlled, leading to a heterogeneous particle size distribution. We therefore explored the influence of ternary solvent systems combining water, the short-chain alcohol (2-propanol) and either oleyl alcohol or 2-octanol (the latter added at 1% (v/v) of the total reaction volume).

Structural and Morphological Analyses: All nanoamanufacturaed materials were examined by transmission electron microscopy (TEM) was carried out using a FEI Tecnai G^2Sphera Microscope. Samples were suspended in alcohol for deposition on the EM grids. The nanoamanufacturaed materials were examined by Scanning electron microscopy (SEM) using a FEI XL40 Sirion FEG Digital Electron Scanning Microscope. BET surface areas were measured with nitrogen

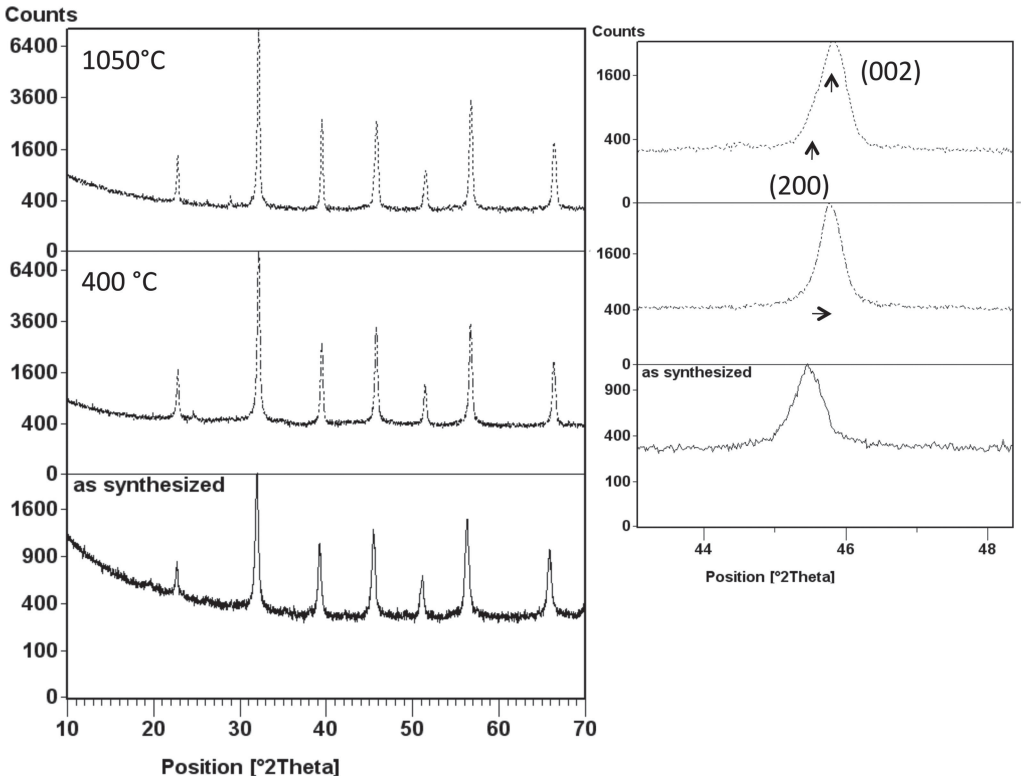

Figure 4. (Left) XRD of the $BaTiO_3$ as a function of sintering; (bottom) as obtained directly from the reactor, (Middle) after sintering at 400 °C, and (top) after sintering at 1,050 °C, respectively, (Right) The shift to tetragonal structure upon sintering as indicated by the shift and diffuse splitting of the reflection at (200) into (002) and (200).

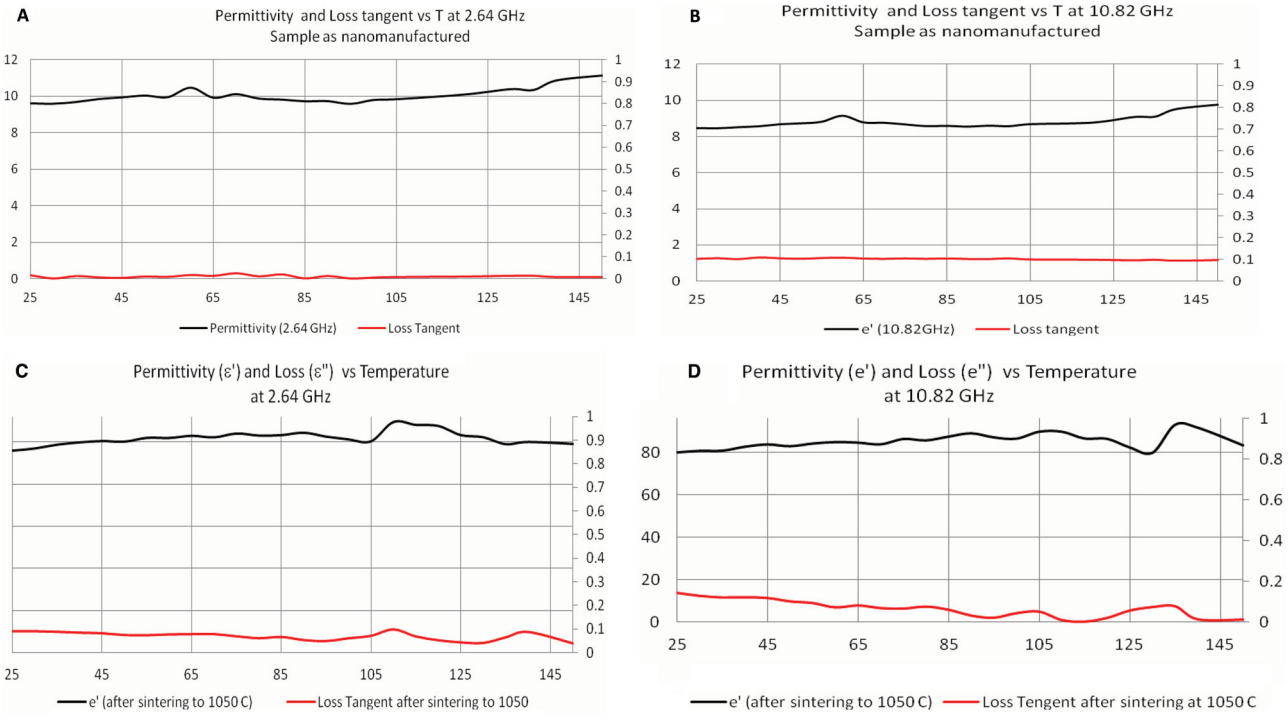

Figure 5. A,B) Permittivity and loss tangent for the material as-made and C,D) after sintering to 1050 °C. These data confirm low loss material as also indicated by the flat loss tangent curves. In the case of the as-made material, the low permittivity is due primarily to the centrosymetric cubic structure.

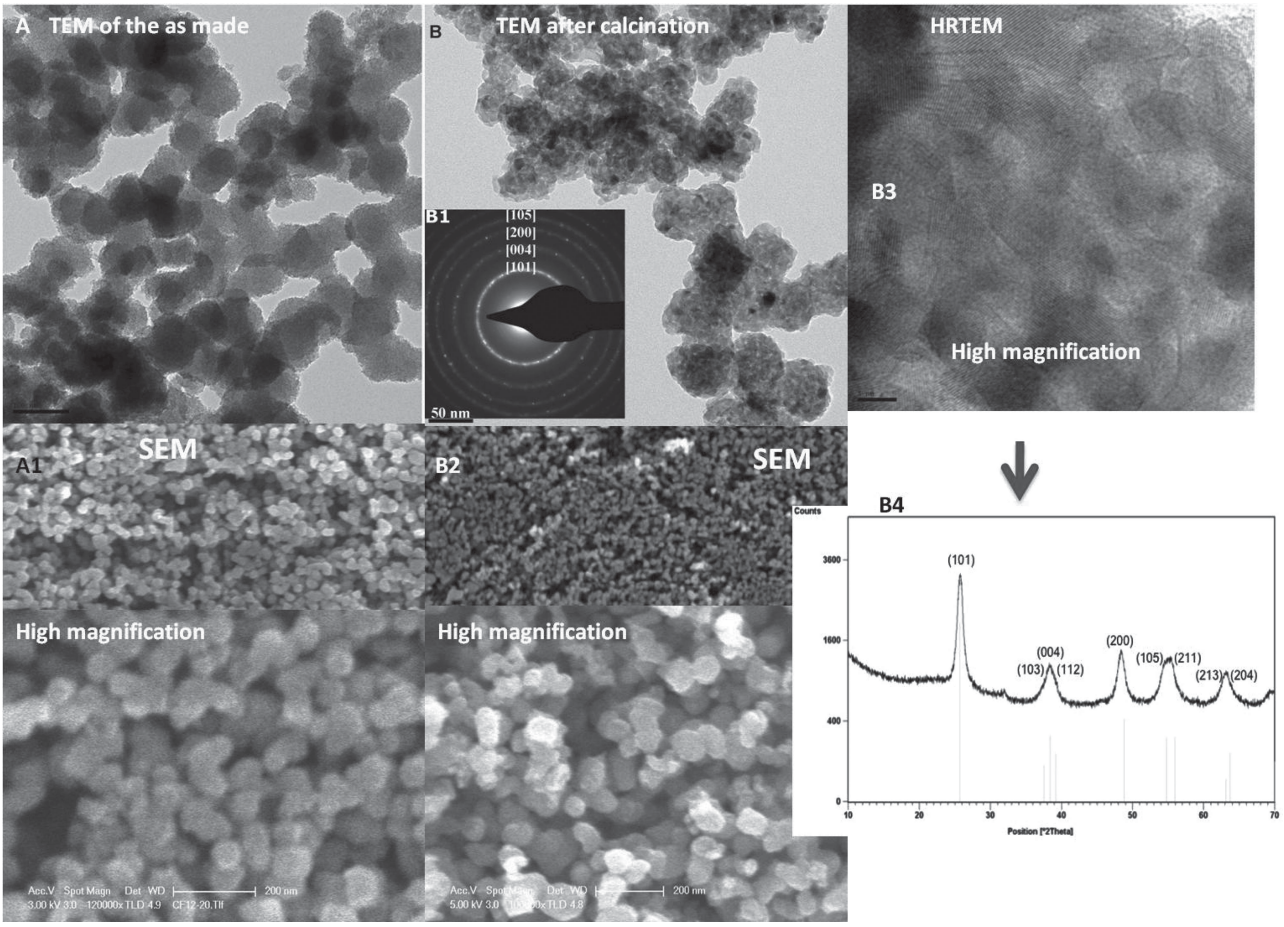

Figure 6. A,A1) TEM and scanning electron microscopy (SEM) images of the amorphous TiO_2 mesoporous nanosponges as made (roughly spherical particles are in the range of 60–80 nm). B,B2) After sintering at 400 °C for 2 h (spherical particles remain in the range of 60–80 nm). B3) HRTEM of one nanosponge particle; size within each agglomerate is ca. 9 nm as determined from the Scherrer relationship, and 10–12 nm from the HRTEM images. SAED pattern (B1 insert) and B4) XRD showing high purity anatase matching JCPDS reference card 01–075–1537; diffraction peaks of the reference phase are indicated as vertical lines.

adsorption at the boiling point of 77 K using a BET porosimeter (TriStar, Micromeritics). From the model developed by Brunauer, Emmet, and Teller in 1940s, the specific surface area of the porous carbons was determined. Pore size distributions were calculated by the Barrett-Joyner-Halenda (BJH) method. X-ray diffraction was carried out using (XRD) (X'PERT powder diffractometer (CuKα radiation)). The Cu Kα tube was operated at 45 kV and acurrent of 40 mA. The particle size is estimated using Scherrer equation $d = K*\lambda/\cos\theta*A$, where d is the particle size in nm, K is a shape factor (0.9), λ is the X-ray wavelength = 0.154 nm, θ is the Bragg angle and A is the FWHM in radians. The particle size was calculated from the broadening of the (1 1 0) peak of $BaTiO_3$ or (101) peak in the case of TiO_2.

Permittivity and Loss measurement: The nanopowders were consolidated into pellets of 13 mm in diameter and a thickness of >2 mm. The pellets were analyzed in reflection mode using an Agilent coaxial probe (85070E) connected to a Network Analyzer. The probe was

Table 1. Yield of scale-up.

Material	Yield/24 h [kg]	Droplet size [μm]	Particle size at the exit of the reactor [nm]	Particle size after calcination [nm]
$BaTiO_3$	1.381 (0.959 g/min)	11.8	23–27 nm (XRD)	400 °C; 24 h
			25–35 nm (TEM)	33 nm
			<50 nm (SEM)	
TiO_2	2.923 (2.030 g/min)	11.8	Amorphous (XRD)	400 °C; 2 h
			<10 nm (TEM)	9.8 nm (XRD)
			60–80 nm (SEM)	10–12 nm TEM

calibrated prior to use and the surface of pellets was smooth and flat to avoid any air gap.

Supporting Information

Supporting Information Additional details about the reactor and the nanomanufacturing steps, XRD, BET, TGA, Raman SEM.

Acknowledgements

This work was supported by the US Army Research Office through grant W911NF-09-D-0001 to the Institute for Collaborative Biotechnologies and by UCSB's Center for Energy Efficient Materials, a DOE-supported Energy Frontiers Research Center (contract #DE-SC0001009. D.E.M. was supported by the US Dept. of Energy (DEFG03–02ER46006). Materials characterization was made possible by use of the facilities of UCSB's Materials Research Laboratory (through the NSF's MRSEC Program grant no. DMR05–20414). The authors thank Prof. Michael F. Doherty for helpful discussion, and R. Bock and Jon Suen for their excellent assistance.

Received: June 5, 2013
Revised: July 21, 2013
Published online: November 11, 2013

[1] a) National Science and Technology Council, "*A National Strategic Plan For Advanced Manufacturing*", Office of Science and Technology Policy, February, **2012**. http://www.whitehouse.gov/sites/default/files/microsites/ostp/iam_advancedmanufacturing_strategicplan_2012.pdf, accessed: May, 2012; b) A. M. Richard, *Manufacturing Technol. News* **2012**, *19*, 3, http://www.manufacturingnews.com/news/national-network-for-manufacturing-innovation-228112.html, accessed: April, 2012.
[2] Y. Engel, J. D. Schiffman, J. M. Goddard, V. M. Rotello, *Mater. Today.* **2012**, *15*(11), 478–485.
[3] M. J. Jackson, *Microfabr. Nanomanuf.* **2006**, 367–387.
[4] National Science and Technology Council "National Nanotechnology Initiative Strategic Plan", February, **2011**. http://www.hsdl.org/?view&did=10693, accessed: June, 2011.
[5] *Processing and Upscaling of Nanostructured Materials.* NMP-**2008**–2.1–2 http://www.minos-euro.net/fp7_wp/nmp/nmp_2008.php?nr=8, accessed: May, 2011.
[6] M. R. Pinto, *Future Trends Microelectron.* **2007**, 154–166.
[7] A. Aimable, N. Jongen, A. Testino, M. Donnet, J. Lemaître, H. Hofmann, P. Bowen, *Chem. Eng. Technol.* **2011**, *34*, 344–352.
[8] R. L. Brutchey, D. E. Morse, *Chem. Rev.* **2008**, *108*, 4915–4934.
[9] R. L. Brutchey, D. E. Morse, *Angew. Chem., Int. Ed.* **2006**, *45*, 6564–6566.
[10] B. Schwenzer, K. M. Roth, J. R. Gomm, M. Murr, D. E. Morse, *J. Mater. Chem.* **2006**, *16*, 401–407.
[11] T. Ould-Ely, M. Luger, L. Kaplan-Reinig, M. Doherty, K. Niesz, D. E Morse, *Nat. Protoc.* **2011**, *6*, 97–104.
[12] R. L. Brutchey, G. Cheng, Q. Gu, D. E. Morse, *Adv. Mater.* **2008**, *20*, 1029–1033.
[13] H. M. Jung, J.-H. Kang, S. Y. Yang, J. C. Won, Y. S. Kim, *Chem. Mater.* **2010**, *22*, 450–456.
[14] F. E. Livingston, W. L. Sarney, K. Niesz, T. Ould-Ely, A. R. Tao, D. E. Morse, *Proc. SPIE* **2009**, *7321*, 73210I.
[15] J. Chen, *J. Comput. Theor. Nanosci.* **2011**, *8*, 722–728.
[16] Y. Saito, H. Sato, Y. Sakabe, *J. Chem. Eng. Jpn.* **2008**, *41*(5), 441–446.
[17] D. Bao, K. Z. Rajab, Y. Hao, E. Kallos, W. Tang, C. Argyropoulos, Y. Piao, S. Yang, *New J. Phys.* **2011**, *13*, 103023.
[18] J. S. Capurso, *J. Am. Ceram. Soc.* **1998**, *81*, 337–346.
[19] S. S. Nonnenmann, J. E. Spanier, *J. Mater. Sci.* **2009**, *44*, 5205–5213.
[20] J. F. Scott, *Science* **2007**, *315*, 954.
[21] S. P. Alpay, V. Nagarajan, G. A. Rossetti Jr., *J. Mater. Sci.* **2009**, *44*, 5021–5024.
[22] B. Walch, PCT Int. App., (Robert Bosch GmbH, Germany), **2012**, WO2012062507 (A1) .
[23] H. Hayashi, T. Noguchi, N. M. Islam, Y. Hakuta, Y. Imai, N. Ueno, *J. Cryst. Growth.* **2010**, *312*, 3613–3618.
[24] K. Matsui, T. Noguchi, N. M. Islam, Y. Hakuta, H. Hayashi, *J. Cryst. Growth.* **2008**, *310*, 2584–2589.
[25] H. Reveron, C. Aymonier, A. Loppinet-Serani, M. Maglione, C. Elissalde, F. Cansell, *Mater. Res. Soc. Symp. Proc.* **2005**, *878E (Solvothermal Synthesis and Processing of Materials)*, Y1 5.1.
[26] H. Reveron, C. Aymonier, A. Loppinet-Serani, C. Elissalde, M. Maglione, F. Cansell, *Nanotechnology* **2005**, *16*, 1137–1143.
[27] D. S. Jung, S. K. Hong, J. S. Cho, Y. C. Kang, *J. Eur. Ceram. Soc.* **2007**, *28*, 109–115.
[28] A. Purwanto, W.-N. Wang, I. W. Lenggoro, K. Okuyama, *J. Eur. Ceram. Soc.* **2007**, *27*, 4489–4497.
[29] I. Huang, Z. Jia, I. Kymissis, S. O'Brien, *Adv. Funct. Mater.* **2010**, *20*, 554–560.
[30] Y. Furukawa, C. A. H. A. Mutsaers, PCT Int. Appl. (Koninklijke Philips Electronics N.V., Neth.), **2006**, WO2006067678 (A1) .
[31] X. Wei, G. Xu, Z. Ren, G. Shen, G. Hanw, *J. Am. Ceram. Soc.* **2008**, *91*, 3774–3780.
[32] Z. Shen, S. Li, Z. Liu, J. Zhang, J. Chen, *Chin. J. Chem. Eng.* **2005**, *13*, 225–233.
[33] J. Q. Qi, L. Sun, X. W. Qi, Y. Wang, H. L. W. Chan, *J. Solid State Chem.* **2011**, *184*, 2690–2694.
[34] K. Kiss, J. Magder, M. S. Vukasovich, R. J. Lockhar, *J. Am. Ceram. Soc.* **1966**, *49*, 291–295.
[35] X. Zhao, C. Hinchliffe, C. Johnston, P. J. Dobson, P. S. Grant, *Mater. Sci. Eng., B* **2008**, *151*, 140–145.
[36] M. Zhang, T. W. Karjala, B. W. S. Kolthammer, *Ind. Eng. Chem. Res.* **2007**, *46*, 5922–5935.
[37] M. Tanaka, Y. Makino, *Ferroelectr., Lett. Sect.* **1998**, *24*, 13–23.
[38] S. Wada, A. Yazawa, T. Hoshina, Y. Kameshima, H. Kakemoto, T. Tsurumi, Y. Kuroiwa, *IEEE Trans. Ultrason. Ferroelectr. Freq. Control* **2008**, *55*, 1895–1899.
[39] X. Chen, L. Liu, Z. Liu, M. A. Marcus, W.-C. Wang, N. A. Oyler, M. E. Grass, B. Mao, P.-A. Glans, P. Y. Yu, J. Guo, S. S. Mao, *Sci. Rep.* **2013**, *3*, 1510.
[40] X. Chen, L. Liu, P. Y. Yu, S. S. Mao, *Science* **2011**, *331*, 746–750.